# VICTORIA UNIVERSITY
## MELBOURNE AUSTRALIA

*Identification of material and physical features of membrane distillation membranes for high performance desalination*

This is the Published version of the following publication

# Identification of material and physical features of membrane distillation membranes for high performance desalination

Jianhua Zhang, Noel Dow, Mikel Duke, Eddy Ostarcevic, Jun-De Li, Stephen Gray*

*Institute of Sustainability and Innovation, Victoria University, PO Box 14428, Melbourne, Victoria 8001, Australia (E-mail: stephen.gray@vu.edu.au)*

**Abstract**

In this paper, the performance of various membranes were assessed in direct contact membrane distillation (DCMD) under different feed velocities and inlet temperatures. The membranes studied included a polyvinylidenefluoride (PVDF) microfiltration membrane with a non-woven support layer, a polytetrafluoroethylene (PTFE) microfiltration membrane with a non-woven support layer, and three MD membranes made from PTFE of different pore size and all with a structured scrim support layer. The results showed that distillation using PTFE membranes produced much higher flux than that of the PVDF microfiltration membrane at the same operational conditions, and the support layer affected not only the flux, but also the energy efficiency (0.51 – 0.24). The results also show that increasing the velocity of the feed and its inlet temperature increased the flux, but the rate of flux increase diminishes at high velocities. The mass transfer coefficient improved for thinner support and active layer membranes, leading to fluxes as high as 46 $L.m^{-2}h^{-1}$ at 80˚C. The heat transfer characteristics were found to be superior for the open scrim backed membranes compared to the non-woven support membranes, resulting in significantly greater thermal efficiency for the scrim backed membranes.

**Keywords**
Membrane distillation; water treatment; desalination; direct contact membrane distillation

## 1. Introduction

Membrane Distillation (MD) is a membrane-based water treatment process where the driving force for MD is a vapour pressure difference across the membrane. This differs from reverse osmosis (RO) where the absolute pressure difference is the driving force for mass transfer.

Membrane distillation (MD) has been known for many years, but its commercial implementation has been hampered by low water fluxes and the need for low cost heat sources. With greater emphasis being placed on energy efficiency, MD coupled with waste heat or solar heat sources to drive the process is being reconsidered. In particular, the use of MD to treat brine concentrates is receiving renewed attention for its benefits of increased water recovery and lower brine discharges, largely due to the independence of driving force from salinity. Due to recent advancements in membrane technology, better performing membranes have become available and the features of these materials linked to improved fluxes and salt rejection rate have yet to be identified.

In comparison with other membrane separations, MD has several advantages including very high rates of rejection rate for non-volatile components, lower operating pressure than pressure-driven membrane processes, much larger membrane pore size than that of RO (and typically larger than that of ultra-filtration membranes), less sensitivity to fouling than RO, reduced vapour space compared to conventional distillation, low sensitivity to feed salinity and low feed temperature requirements (40-80°C) [1]. The MD process is capable of treating highly concentrated wastewater and utilising low-grade heat for water distillation. It is a promising technique for minimising RO concentrate discharge, and for desalination and wastewater recycling in places where waste heat, solar or geothermal sources are available [2].

Hydrophobic materials, such as polypropylene (PP), PTFE, PVDF, etc., can be used to fabricate MD membranes [3]. In this paper, PVDF and PTFE membranes were employed. The surface

energies of PTFE and PVDF are 9.1 and 30.3 kN/m, respectively, so both materials have high hydrophobicity [4]. They also have thermal conductivities as low as 0.22-0.45 $Wm^{-1}K^{-1}$ and good chemical stability at the operating temperature of membrane distillation [5]. Their pore sizes are in general in the range of 0.2 to 1.0 μm and thicknesses are in the range of 0.06 to 0.25 mm [6]. Depending on the conditions and structures, the reported fluxes of PTFE and PVDF flat sheet membranes are generally in the range of 5-60 $Lm^{-2}h^{-1}$ and 4-40 $Lm^{-2}h^{-1}$ [5, 7-10], respectively, in direct contact membrane distillation. Specific membranes for MD have been fabricated [11], however, these materials are not commercially available as yet [12].

The cost of desalination by MD using waste heat has been estimated by Meindersma, et. al [13] to be \$0.31/$m^3$. While this figure seems optimistic, it does suggest that desalination via MD could be cost competitive with conventional processes. In this paper, we will study membranes with different characteristics to identify features that lead to enhanced flux.

### 1.1. MD configurations

In MD processes, one side of the membrane is in contact with liquid feed. How the permeate side of the membrane is configured can vary, and four MD configurations have been identified: Direct Contact Membrane Distillation (DCMD), Air Gap Membrane Distillation (AGMD), Vacuum Membrane Distillation (VMD) and Sweep Gas Membrane Distillation (SGMD) [5]. For the purpose of desalination, the DCMD configuration was employed in this paper because it is simple to perform in the laboratory, has the least process parameters and high water flux. DCMD is therefore well suited to compare the performance of different MD membranes for desalination, particularly given the higher flux and reduced mass transfer resistance on the permeate side compared to the other forms of MD.

### 1.2. Heat transfer and mass transfer in DCMD

To identify features of membranes that could enhance MD performance, the heat and mass transfer processes must be described. Figure 1 shows the heat and mass transfer processes in DCMD. The feed temperature ($T_f$) drops across the boundary layer on the feed side to $T_1$. The permeate temperature $T_p$ increases across the permeate boundary layer to $T_2$. The vapour pressure difference across the membrane depends on the temperature $T_1$ and $T_2$, and the driving force is therefore $P_{T1}$ - $P_{T2}$ where $P_{T1}$ and $P_{T2}$ are the vapour pressures at $T_1$ and $T_2$, respectively. The feed concentration $C_f$ increases across the feed boundary layer to $C_1$ [8, 14].
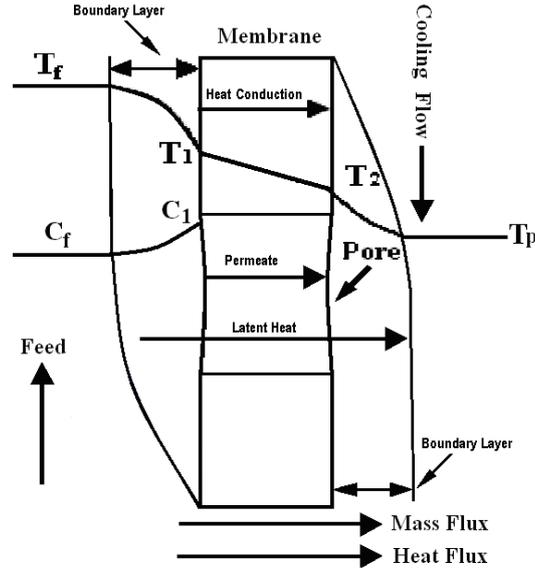
Figure 1. Heat and mass transfer through membrane

*1.2.1 Heat transfer*

In DCMD, the driving force for mass transfer is the vapour pressure difference that arises from the temperature difference between the liquid phases on both sides of the membrane. Thus, DCMD performance relies on the complex relationships between simultaneous heat and mass transfers, which are in the same direction from the feed side to the permeate side. Assuming no heat loss through module walls, the total heat flux can be expressed as [15, 16]:

$$Q = \alpha_1(T_f - T_1) = H_{latent}N + \frac{\lambda}{b}(T_1 - T_2) = \alpha_2(T_2 - T_p) \tag{1}$$

where $\alpha_1$ and $\alpha_2$ are the heat transfer coefficients on hot side and cold side respectively, $\lambda$ is the thermal conductivity of the membrane, $b$ is membrane thickness, $N$ is the vapour flux through the membrane, and $H_{latent}$ is the latent heat of vaporisation for water. In Eq. (1), $\lambda(T_1-T_2)$ is the sensible heat transfer across the membrane and $H_{latent}N$ is the latent heat transfer. The heat conduction coefficient $\lambda$ can be calculated as [15, 16]

$$\lambda = (1-\varepsilon)\lambda_{solid} + \varepsilon\lambda_{air} \tag{2}$$

where $\lambda_{solid}$ and $\lambda_{air}$ are thermal conductivities of air and solid, respectively, and $\varepsilon$ is the membrane porosity.

*1.2.2 Mass transfer*

Mass transfer in the DCMD process includes five main steps. These are water molecules: diffuse from the bulk feed into the boundary layer, vaporise from liquid/gas interface of the feed, pass through membrane pores, condense at the liquid/gas interface of the permeate side and diffuse into the bulk permeate.

The mass transfer model of membrane distillation suggests that the mass transfer rate or water flux is proportional to vapour pressure difference across the membrane [17].

$$N = C(P_{T_1} - P_{T_2}) = C\Delta P \tag{3}$$

where $C$ is the mass transfer coefficient that can be obtained experimentally. The flux should change with temperature exponentially, because vapour pressure is an exponential function of temperature [18]. According to [9, 15], it can be estimated as

$$C \propto \frac{r^a \varepsilon}{bt} \tag{4}$$

where $r$ is the nominal pore size of membrane, $a$ is the exponent of $r$ in the range of 1 to 2 and $t$ is the pore tortuosity.

$C$ is an important parameter to assess the performance of a membrane as its value depends on the mass transfer characteristics of the membrane. However, it is difficult to accurately measure the temperature at the interface between the vapour phase and liquid phase experimentally. Therefore, in our study, the performances of different membranes were compared under the same hydrodynamic and thermal conditions and subsequently under the same boundary layer conditions. A global mass transfer coefficient $C_g$, calculated from the bulk temperatures and which includes mass transfer phenomena in the boundary layer, was used to assess MD membranes.

## 1.3. Membrane characteristics

From the above mass transfer and heat transfer equations, membranes that are most suitable for membrane distillation processes should have the following properties [1]:
- Small thickness and low tortuosity
- Low thermal conductivity of membrane material, so that heat loss due to sensible heat transfer can be minimized
- High porosity to lower conductive heat flux and increase the water vapour transport coefficient through the membrane
  Reasonably large pore size, limited by membrane wetting that will occur when the interfacial pressure difference $\Delta P_{interface}$ is greater than the minimum membrane Liquid Entry Pressure (LEP)

$$\Delta P_{interface} = P_{liquid} - P_{gas} \tag{5}$$

$$LEP = \frac{-2B\gamma_l}{r_{max}} \cos \theta \tag{6}$$

  Here, $B$ is a geometric factor, $\gamma_l$ is the surface tension of the solution, $\theta$ is the contact angle between the solution and the membrane surface, $r_{max}$ is the largest pore size of the membrane, $P_{liquid}$ is the pressure of the process liquid and $P_{gas}$ is the gas phase pressure in the pores.
- Low surface energy or high hydrophobicity, so that the membrane is applicable under higher pressure or with bigger pore size.

The early membranes had very poor performance when membrane distillation was invented in the late 1960s. Partly for this reason, membrane distillation was not commercially employed at that time [19]. In the 1980s, membranes with improved characteristics became available, and MD research rose again [20]. However, in recent times membranes with even greater improved characteristics have become available. In this paper, recently available MD membranes were investigated through their physical structures, and performance tests for flux, energy efficiency and salt rejection under different operational conditions. Using the characteristics identified above, we will show how the membrane materials and physical features lead to the observed measures of flux and rejection. We will in turn provide some guidance to further improve the performance of MD membranes.

## 2. Experimental method

### 2.1. Membranes and their properties

Table 1 lists the five membranes used in the experiments. The two supported by a non-woven fabric layer were microfiltration (MF) membranes, and the other three supported by a scrim were membranes designed for MD. The properties presented in Table 1 were provided by the manufacturers.

Table 1
Properties of membranes as provided by the manufacturers

| Membrane | Material of active layers | Support layer | Nominal pore size (µm) | Provider |
|---|---|---|---|---|
| $M_{mt1.00}$ | PTFE | Nonwoven fabric | 1.00 | Membrane Solutions |
| $M_{p0.30}$ | PVDF | Nonwoven fabric | 0.30 | GE Osmonics |
| $M_{gt0.22}$ | PTFE | Scrim | 0.22 | GE Osmonics |
| $M_{gt0.45}$ | PTFE | Scrim | 0.45 | GE Osmonics |
| $M_{gt1.00}$ | PTFE | Scrim | 1.00 | GE Osmonics |

*Contact angle measurement*

Contact angles were measured as an indicator of hydrophobicity. The contact angle of membrane samples were assessed by a KSV contact angle meter (CAM200) equipped with a video capturing system. Static contact angles were measured by the sessile drop method. An 8 µL drop was formed on the flat surface of the membrane using a syringe, and the contact angle of each membrane was measured 2-3 times.

*SEM characterisation*

To observe their cross sections, the membranes were frozen in liquid nitrogen and then cut with a blade. Membrane active layer thicknesses were measured by a LEICA SEM (S440 W) via imaging of the cross section of the membrane. The thickness of each membrane was measured three times from different sections of the membrane contained in one image, and an average thickness was reported as the membrane thickness.

*Porosity measurement*

The porosity was determined by mass difference. The sizes of the prepared samples were in the range of 30-38 mm×45-63 mm. The weights of each membrane with its support and the support layer without the active layer were measured by an A&D balance (HR-200). The porosity of membrane active layer was calculated by

$$\varepsilon = 1 - \frac{(m_{total} - m_{support})/\rho}{V} \tag{7}$$

where $\rho$ is the material density of the active layer, in which a midpoint in density range of the reported polymer density [21, 22] was used (an error less than 3%); $m_{total}$ and $m_{support}$ are respectively the masses of the membrane with the support layer and the support layer only; $V$ is the volume of active layer, which was calculated by multiplying the area with the active layer thickness. The porosity of the support layer was worked out similarly. The surface porosity can be estimated by

$$\varepsilon_{surface} = \frac{\varepsilon}{t_{avg}} \qquad (8)$$

where $\varepsilon_{surface}$ is the surface porosity, and $t_{avg}$ is the average tortuosity of the pore.

*LEP measurement*

LEP was measured by conductivity changes and Figure 2 shows a schematic diagram of the apparatus. A salt solution was forced through the membrane as the pressure on the salt solution side was gradually increased, and the LEP detected by an increase in conductivity on the permeate side. A Millipore filter holder (sx0002500, diameter=25 mm) was used to secure the membrane, and the holder cavity was filled with 20% NaCl solution. The holder was submerged in 200 mL deionised water in a beaker, and the deionised water was brought into contact with the membrane support layer. Having the membrane in contact with the deionised water and stirring the deionised water with a magnetic stirrer increased the diffusion rate of salt into the bulk water, so that an increase in conductivity could be detected when the LEP was exceeded. A HANNA HI 9032 conductivity meter was used to monitor changes in conductivity of the deionised water, and it was estimated from the sensitivity of this conductivity meter that 0.05 µL of 20% NaCl could be detected in the deionised water. The pressure of the salt solution was increased in increments of 5 kPa, and the pressure was maintained for one minute before the next 5 kPa pressure increase was implemented. The LEP was equal to the pressure at which a conductivity increase in the deionised water was detected.

According to [23], the contact angle between the liquid and hydrophobic membrane only changes slightly with concentration variation, and contact angle can be corrected for variations in salt concentration via changes in surface tension. The water surface tension varies with salt concentration and can be calculated by [24]

$$\gamma_l = \gamma_0 + \frac{\Delta\gamma}{\Delta C_{solution}} C_{solution} \qquad (9)$$

where $\gamma_0$ is the surface tension of pure water and equals 72.0 mN/m at 25ºC, the value of $\Delta\gamma/\Delta C_{solution}$ is 1.467±0.05 for NaCl solutions [24], and $C_{solution}$ is the salt concentration. The measured LEP was converted to the LEP of the membrane under experimental condition (1% NaCl solution) via Eqs. (6) and (9).
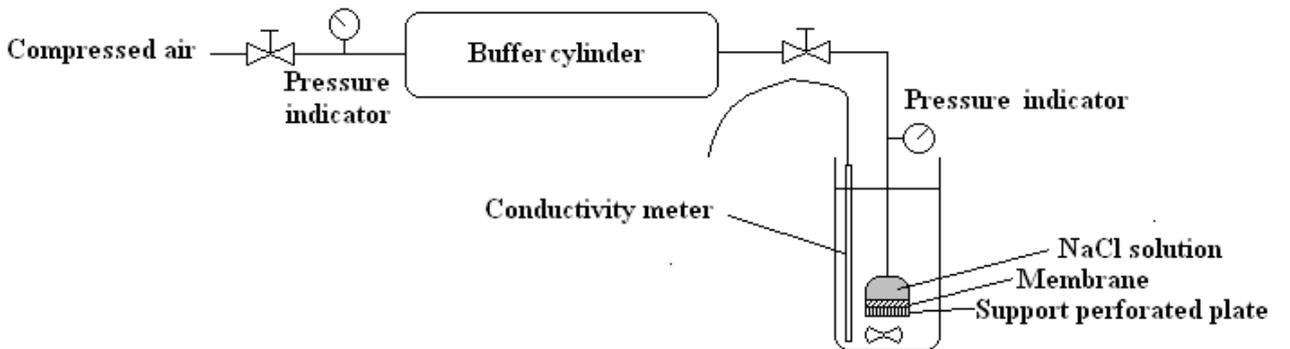


Figure 2. Schematic diagram of LEP test

## 2.2 DCMD Testing

Figure 3 shows a schematic diagram of the counter-current DCMD experimental apparatus. A flat-sheet DCMD configuration with an area of 0.014 m$^2$ was used to evaluate the performance of the five membranes listed in Table 1. The velocities on both sides of the membrane were maintained equal and were controlled by two peristaltic pumps, one for the hot feed and the other for the cold stream. The speed was varied in the range of 0.17-0.36 m/s. The temperature of the feed water was controlled by a heater and was varied in the range of 45-70°C. A chiller was used to cool the cold stream so that it could be recycled and remain at a constant temperature. The cold stream into the DCMD was set at 20°C. The brine feedwater was prepared by dissolving 100 g NaCl into 10 L water (10 g.L$^{-1}$). Water for the hot feed and the cooling fluid were both deionised. The temperature and pressure of the feed and permeate were monitored at their respective inlets and outlets, and a conductivity indicator was used to measure the salt rejection. Spacers provided by GE Osmonics were used on both sides of the membrane to enhance the turbulence of the stream and to provide support to the membrane. The flux was determined by measuring the weight of the product reservoir over time. Our experimental results show that the flux of the new membranes was about 15-20% higher than that of the conditioned membranes under the same operating conditions. After the membrane was used for 5-8 hours, the flux became stable and its variation was in the range of 5-10%. In the present experiments, all data were obtained from conditioned membranes with stable flux, and the reported flux is the mean value measured every hour over a 4-6 h period. All the results presented for an individual membrane type were measured from the same membrane piece, and the error in the flux was ±5-10%. Error bars are not shown later in Figures 5-8 for the sake of clarity.
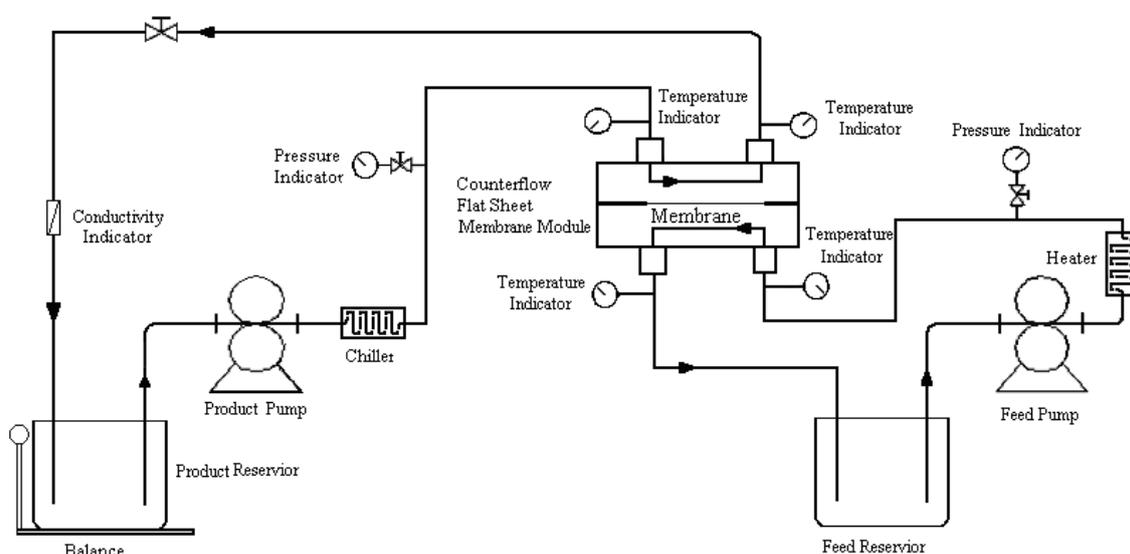


Figure 3. Schematic diagram of the experimental setup

## 3. Results and discussion

### 3.1. Membrane properties

Figure 4 shows the SEM images of the support layers and active layers. Images 4a and 4b are the typical structures of non-woven fabric support and scrim support layers. Images 4c and 4d are the typical structures of PVDF active layer and PTFE active layer, respectively. From these images, it

can be seen that the tortuosities of the nowoven fabric support layer should be greater than 1, and that of the scrim support layer should be close to 1.
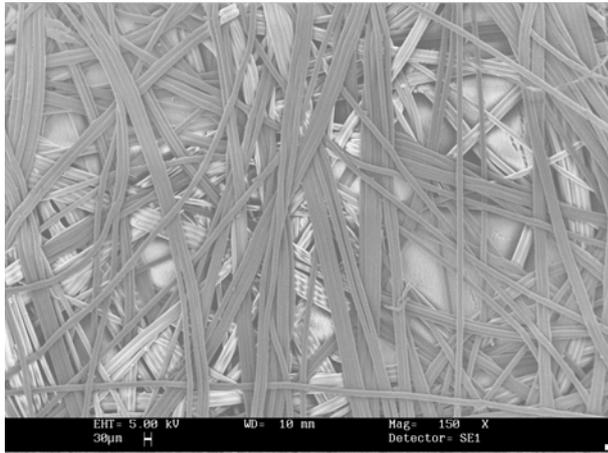


a. non-woven fabric support layer of $M_{mt1.00}$
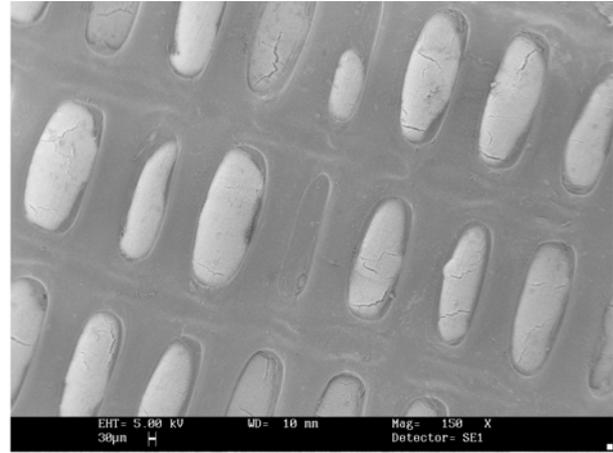


b. Scrim support layer of $M_{gt1.00}$
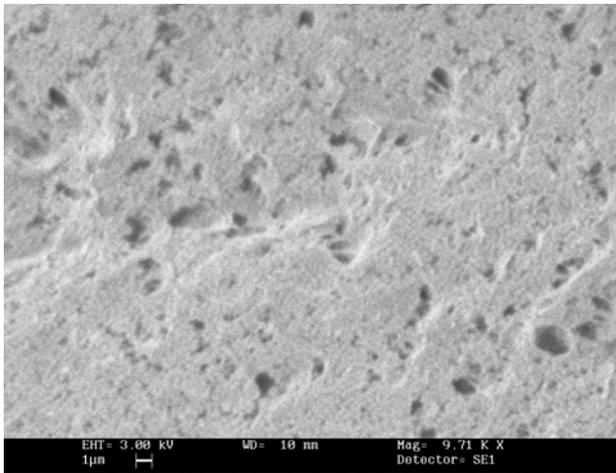


c. Active layer of $M_{p0.30}$
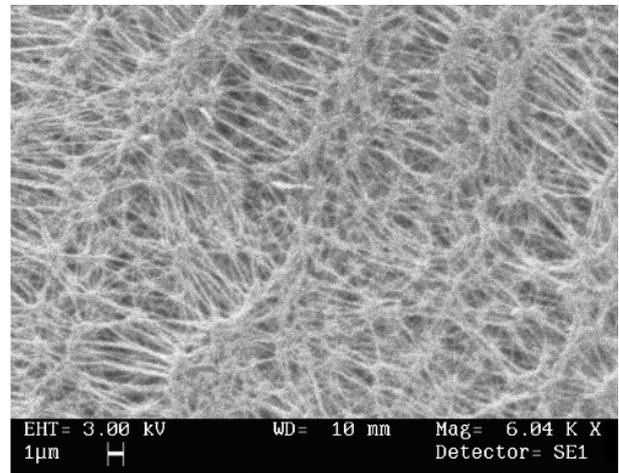


d. Active layer of $M_{gt0.22}$

Figure 4. SEM images of support and active layers

Table 2
Measured and calculated properties of membrane

| Membrane | Thickness (µm) | | Contact angle | LEP of membrane (kPa) | | Porosity of active layer (%) | Porosity of support layer (%) | |
|---|---|---|---|---|---|---|---|---|
| | Total | Active layer | Active layer | Measured | Converted | Bulk | Bulk | Surface |
| $M_{mt1.00}$ | 215 | 30 | 126°±5 | 24.0±2.5 | 21.8±2.5 | 92.9 | 68.3 | ≤68.3 |
| $M_{p0.30}$ | 234 | 90 | 113°±5 | 21.3±2.5 | 19.4±2.5 | 81.0 | 25.6 | ≤25.6 |
| $M_{gt0.22}$ | 174 | 77 | 144°±5 | 154.0±2.5 | 140±2.5 | 83.1 | 70.0 | 70.0 |
| $M_{gt0.45}$ | 164 | 67 | 144°±5 | 90.8±2.5 | 82.5±2.5 | 87.8 | 70.0 | 70.0 |
| $M_{gt1.00}$ | 127 | 30 | 150°±5 | 47.8±2.5 | 43.5±2.5 | 89.4 | 70.0 | 70.0 |

Figure 4 and Table 2 show that the PTFE active layers are more porous than the PVDF membrane and the scrim support layer can provide more open area for vapour transport than that of the non-woven fabric support layer. Furthermore, the $M_{gt}$ membranes have larger contact angles, smaller overall thicknesses, and higher LEP. According to the characteristics listed in Table 2, and Eqs. (2),

(4) and (6), $M_{gt}$ membranes should have low thermal conductivity and mass transfer resistances, and can be employed under relatively high pressure conditions.

*3.2 Membrane fluxes and global mass transfer coefficients at different velocities*

Figure 5 shows the measured fluxes for hot side temperatures of 60°C and cold side temperatures of 20°C for the five membranes listed in Table 1. Permeate fluxes rose as the feed velocity increased for all the five membranes, because high velocity means high turbulence which will result in less temperature polarisation and increased driving force across the membrane. However, the rate of flux increase slowed at higher feed velocities (ie. the curves approach constant values). Similar asymptotic trends of permeate flux with increasing feed velocities were reported previously [25, 26]. $M_{gt1.00}$ showed the best performance at all velocities, and achieved the highest flux of 26.2 $Lm^{-2}h^{-1}$ at the hot feed velocity of 0.36 m/s. The lowest flux was from $M_{p0.30}$, and its highest flux at the hot feed velocity of 0.36 m/s was only around half that of the lowest flux of the novel PTFE membrane $M_{gt1.00}$ at the hot feed velocity of 0.17 m/s. $M_{gt1.00}$ showed higher flux than $M_{gt0.45}$ at all hot feed velocities, and $M_{gt0.45}$ had higher fluxes than $M_{gt0.22}$ at all velocities. Although $M_{mt1.00}$ has a higher active layer porosity and larger nominal pore size than those of $M_{gt0.45}$, its average flux in the tested flowrate range was about 50% less than that of the $M_{gt0.45}$. This suggests that the more porous and open support layer of the $M_{gt0.45}$ membrane leads to the higher flux relative to the non-woven support layer of the $M_{mt1.00}$ membrane, and this is discussed later.

**Hot Side 60°C-Cold Side 20°C**
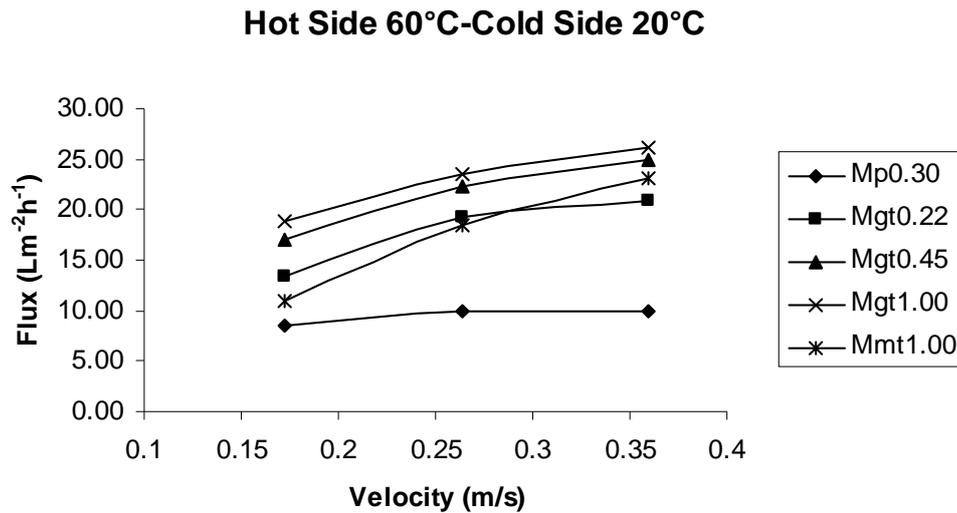


Figure 5. Relation between flux and velocity

During the DCMD experiments, both the level of turbulence and temperature differences across the membrane rose when the velocities were increased. To avoid the influence of higher temperature difference on flux in characterising the membrane properties, a global mass transfer coefficient $C_g$ was calculated using Eq. (3). To do so, an average $\Delta P_{avg}$ for counter current flow was calculated from

$$\Delta P_{avg} = \frac{(P_{fi} - P_{po}) - (P_{fo} - P_{pi})}{\ln[(P_{fi} - P_{po})/(P_{fo} - P_{pi})]} \tag{10}$$

where $P_{fi}, P_{fo}, P_{pi}$ and $P_{po}$ are the vapour pressures respectively at inlet and outlet temperatures of the hot side and cold side. The global mass transfer coefficient includes mass transfer in both the boundary layers and the membrane pores, which will vary with the turbulence state of the stream and is different from the local membrane mass transfer coefficient that is only determined by membrane properties showed in Eq. (4). Assuming the mass transfer coefficients in the boundary

layer are equal under the same hydraulic conditions in the experimental temperature range, the global mass transfer coefficient can be used to make a comparison of mass transfer performance among the different membranes. Based on this assumption, the mass transfer coefficients were calculated and the results are shown in Figure 6.

## Hot Side 60°C-Cold Side 20°C
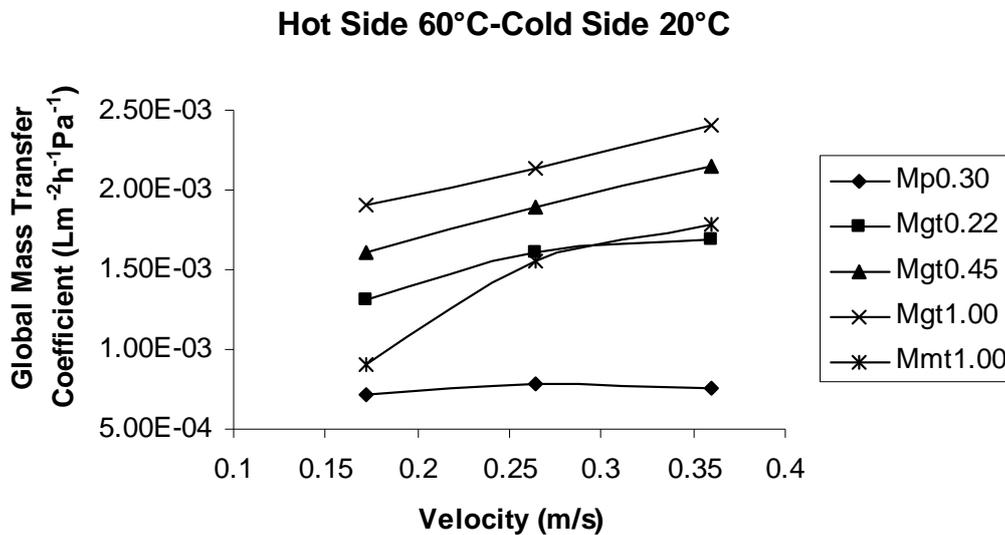


Figure 6. Mass transfer coefficients with respect to feed velocity

Figure 6 shows that $M_{gt}$ series membranes have significantly higher mass transfer coefficients than the other membranes. Although $M_{mt1.00}$ has the same nominal pore size as $M_{gt1.00}$, it only has a mass transfer coefficient similar to that of $M_{gt0.22}$ in the tested velocity range. The $C_g$ of $M_{p0.30}$.was the lowest and was not sensitive to velocity changes, indicating that the mass transfer resistance in the membrane dominates that of the boundary layers.

In Figure 5 and 6, the flux curves of the $M_{mt1.00}$ and $M_{gt0.22}$ intersect each other, which could be caused by the structure of their support layers. Figures 4a and 4b and Table 2 showed that the tortuosity and thickness of the non-woven fabric support layer were greater than those of the scrim support layer, so the non-woven fabric layer may trap more static water and cause a greater degree of temperature polarisation than the scrim support layer at lower flowrate. Therefore, flux gained from membrane supported by non-woven fabric may show stronger dependency on flowrate. At a low flowrate when the boundary layer or temperature polarisation has more influence on flux, $M_{mt1.00}$ showed lower flux than that of $M_{gt0.22}$, while at a high flowrate when turbulence reduces the temperature polarisation effect on flux and flux is mainly controlled by the properties of active layer, $M_{mt1.00}$ showed higher flux than that of $M_{gt0.22}$.

Figure 7 shows the salt rejection rate with respect to velocity for the five membranes listed in Table 1. The pressure drop along the membrane was in the range of 8-20 kPa at these velocities. Salt rejection rates of all the PTFE membranes were more than 99%, regardless of the velocities. Although salt rejection rate of the $M_{p0.30}$ was more than 99% at the low velocity, it reduced to 96% as the velocity increased to 0.36 m/s. This can be attributed to pressure variation in the range of 10-20 kPa at this flowrate, and from Table 2 it can be seen that the LEP of $M_{p0.30}$ was only 19.4±2.5 kPa, which may have allowed wetting to occur under fluctuating pressures at high velocities.

**Hot Side 60°C-Cold Side 20°C**
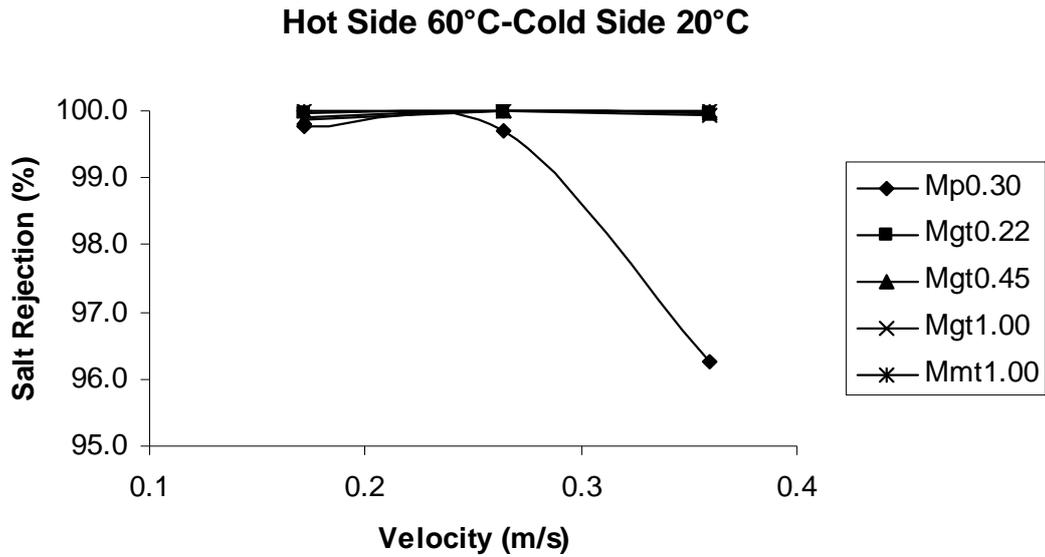


Figure 7. Salt rejections related to feed velocity

*3.3. Temperature influence on membrane flux and energy efficiency*

As $M_{mt1.00}$ and $M_{gt1.00}$ membranes showed the highest flux for a non-woven backed and a scrim backed layers, they were selected for further testing at different temperatures. The permeate fluxes of both membranes increased as the temperature rose. Figure 8 shows the flux at different hot side inlet temperatures at a feed velocity of 0.36 m/s. Although the active layers of these two membranes were made from the same material, with the same nominal pore size, same measured active layer thickness and having similar support layer porosities, $M_{gt1.00}$ showed consistently higher flux than that of $M_{mt1.00}$. The highest flux of 46.3 L m$^{-2}$h$^{-1}$ was achieved from $M_{gt1.00}$ at 80ºC. The difference in flux between these membranes was probably due to the difference in support layers used. From Table 2 and Figure 4, it can be seen that the scrim support layer is thinner and more open (more surface porosity) than the non-woven fabric support layer. Thus, the $M_{gt1.00}$ has a smaller overall thickness and a larger exposed effective area of the active layer than that of the $M_{mt1.00}$ membrane.

**Velocity 0.36 m/s**
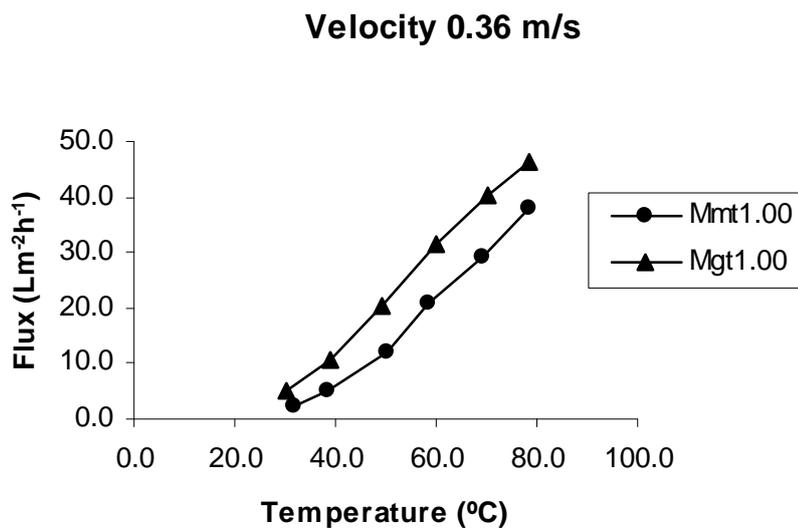


Figure 8. Variation of flux with hot side inlet temperature at a constant velocity

Table 3
Sensible heat transfer and latent heat transfer at different temperatures

| Temperature (ºC) | $M_{mt1.00}$ | | | | $M_{gt1.00}$ | | | |
|---|---|---|---|---|---|---|---|---|
| | Total feed heat loss $Q$ (kW·m$^{-2}$) | Latent heat transfer $H_{latent}N$ (kW·m$^{-2}$) | Sensible heat transfer $\lambda/b \cdot (T_1 - T_2)$ (kW·m$^{-2}$) | Global heat transfer coefficient $U$ (kW·m$^{-2}$K$^{-1}$) | Total feed heat loss $Q$ (kW·m$^{-2}$) | Latent heat transfer $H_{latent}N$ (kW·m$^{-2}$) | Sensible heat transfer $\lambda/b \cdot (T_1 - T_2)$ (kW·m$^{-2}$) | Global heat transfer coefficient $U$ (kW·m$^{-2}$K$^{-1}$) |
| 30 | 12.9 | 1.1 | 11.8 | 164.1 | 12.3 | 3.0 | 9.3 | 135.5 |
| 40 | 19.2 | 3.1 | 16.1 | 151.3 | 21.3 | 6.7 | 14.6 | 123.6 |
| 50 | 31.1 | 7.5 | 23.7 | 136.9 | 32.9 | 12.8 | 20.2 | 110.2 |
| 60 | 39.8 | 10.4 | 29.3 | 132.9 | 45.3 | 19.8 | 25.5 | 101.4 |
| 70 | 56.6 | 18.3 | 38.2 | 121.6 | 49.5 | 25.3 | 24.2 | 87.9 |
| 80 | 69.3 | 23.7 | 45.6 | 118.5 | 59.2 | 28.7 | 30.5 | 92.8 |

The results listed in Table 3 were calculated using Eq. (1). From this table, it is found that the feed heat loss increased when the temperature was higher, and the heat loss due to the latent heat transfer increased faster than that due to the sensible heat transfer, except for the $M_{gt1.00}$ when the temperature increase from 70 to 80ºC. Although $M_{mt1.00}$ is thicker than $M_{gt1.00}$, the global heat transfer coefficient ($U$) of $M_{mt1.00}$ is greater than that of $M_{gt1.00}$ under the same conditions. This means that more heat was wasted in the process when $M_{mt1.00}$ was used, and is consistent with the higher sensible heat transfer values for $M_{mt1.00}$.

The degree of temperature polarisation incurred by their support layers was investigated based on two assumptions: the degree of temperature polarisation on the active layer side for both membranes was similar under similar operating conditions, and the support layer could incur a higher degree of temperature polarisation than the active layer. In these experiments, the stream velocities were kept at 0.36 m/s and permeate and feed inlet temperatures were set at 20 and 60°C, respectively. The configuration of the membranes with respect to contact with the feed and permeate sides was varied, such that both the support layer and active layer of each membrane were contacted with feed in different experiments (ie. the membrane was turned over between experiments). From experimental results listed in Table 4, it is shown that in comparison with the active layer contacting the feed, the flux were reduced by 19% and by 3% for $M_{gt1.00}$ and $M_{mt1.00}$, respectively, when their support layers contacted the feed. From Eq. (3) and the exponential relationship between temperature and vapour pressure [18], it can be concluded that the flux shows more dependency on the feed side temperature polarisation than on permeate side temperature polarisation. This result maybe also due to the proportion of the mass transfer resistance of the boundary layer attributed to the total mass transfer resistance. At the experimental velocity, it is noted from Figure 6 that the global mass transfer coefficient of membrane $M_{mt1.00}$ appeared constant, but the mass transfer coefficient of $M_{gt1.00}$ still seemed to be increasing linearly with velocity. Thus, at this flowrate, for membrane $M_{mt1.00}$, the mass transfer resistance of the boundary layer did not have great influence on the flux, while for membrane $M_{gt1.00}$, the boundary layer still attributed a significant proportion of resistance to mass transfer.

This indicates that the active layer is not controlling the resistance in the case of $M_{gt1.00}$ but it is for $M_{mt1.00}$. As both membranes have similar active layer characteristics, we may assume that the resistance of both active layers are similar. However, the lack of influence of flowrate on flux through $M_{mt1.00}$ demonstrates that the resistance of this membrane is controlling the flux under these conditions, and therefore the support layer adds resistance to the overall membrane given the lower flux relative to $M_{gt1.00}$. Furthermore, the lack of influence of having the feed on either side of the active layer or support layer side suggests that the support layer acts as an integral part of the membrane, and that the resistance of the membrane is composed of the resistance of the support layer and the resistance of the active layer in series. In contrast, the support layer of $M_{gt1.00}$

decreases as the exposed active layer area on one side of the membrane, and also affects temperature polarisation via its affect on the hydrodynamics. Therefore, even greater flux through Mgt1.00 might be achieved via increasing the porosity (open area) of the scrim support layer.

Table 4
Flux changed with layer contacted with feed

| Membrane | Feed contacting support layer | | Feed contacting active layer | |
|---|---|---|---|---|
| | Flux (L.m$^{-2}$h$^{-1}$) | Global mass transfer coefficient ($\times 10^{-3}$ L.m$^{-2}$h$^{-1}$Pa$^{-1}$) | Flux (L.m$^{-2}$h$^{-1}$) | Global mass transfer coefficient ($\times 10^{-3}$ L.m$^{-2}$h$^{-1}$Pa$^{-1}$) |
| M$_{mt1.00}$ | 24.7 | 2.12 | 25.5 | 2.17 |
| M$_{gt1.00}$ | 27.1 | 2.28 | 33.5 | 2.80 |

Figure 9 shows the ratio between the heat transfer contributing to water flux (latent heat) and the total feed heat-loss in the module at different temperatures. The ratio is defined as

$$E = \frac{H_{latent} N \cdot A}{\dot{m}_f \cdot C_p (T_{fi} - T_{fo})} \tag{11}$$

where $A$ is the membrane area, $C_p$ is the specific heat of water, $\dot{m}_f$ is the feed mass flowrate, and $T_{fi}$ and $T_{fo}$ are feed inlet and outlet temperatures respectively. $E$ can be considered as the efficiency of energy used to produce condensate.

These ratios calculated using Eq. (11) represents the effective proportion of energy used for the production of permeate. This ratio is one of the key factors contributing to the operational cost of a MD system, as the more effectively heat can be used to drive the process, the more energy efficient the process will be. Therefore, a higher $E$ indicates more efficient energy use because more fresh water could be produced with the same energy loss.

**Velocity 0.36 m/s**
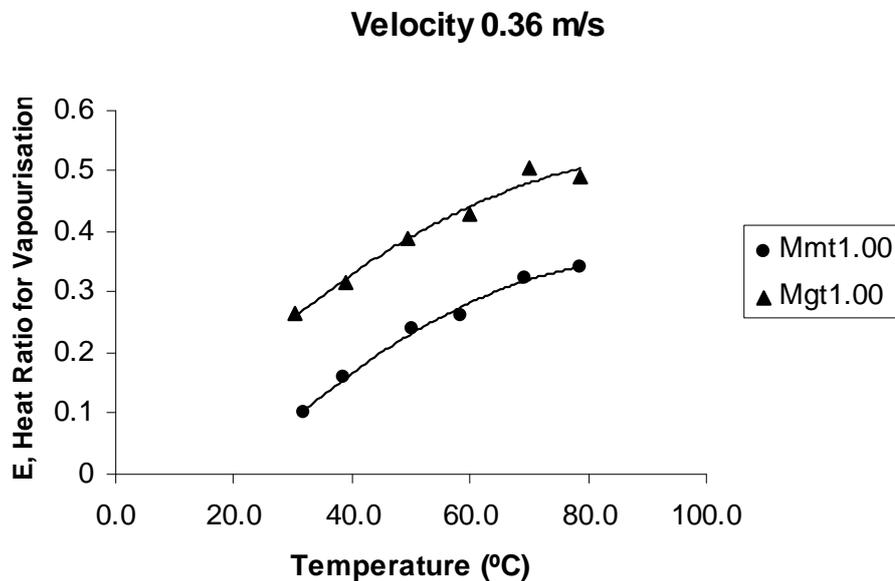


Figure 9. Ratio of heat for water flux to the total feed heat loss, E, at different temperatures

Fig. 9 shows the ratio $E$ for the two membranes. The two curves in Fig. 9 are almost parallel to each other. Over the whole temperature range of 30-80ºC, the average difference calculated at the same temperature was 0.16. For M$_{mt1.00}$, the ratio increased as the temperature rose across the entire temperature range, while for M$_{gt1.00}$, it increased initially, reached a maximum value of 0.50 at 70ºC, and then plateaued between 70ºC and 80ºC. The heat ratio of MD using M$_{gt1.00}$ was 1.4-2.8 times

that of using $M_{mt1.00}$, which means that for the same heat loss in the hot brine stream, the fresh water produced from $M_{gt1.00}$ system was 1.4-2.8 times that of the $M_{mt1.00}$ membrane.

This is a consequence of the more open and lower thickness of the $M_{gt1.00}$ support layer compared to that of $M_{mt1.00}$, and therefore there was less energy transfer associated with the sensible heat passing through the membrane.

*3.4. Key performance features of new generation membranes*

The membranes with the best flux and energy performance have been identified. More hydrophobic membranes appear to result in better salt rejection rate, particularly at higher velocities. Although the scrim support layer seemed to incur a higher degree of temperature polarisation than the non-woven fabric support layer when the flowrate has less effect on the flux, the more open structure of the scrim backing was found to be vital to enhance membrane performance as compared to the non-woven fabric backing, as the scrim backing membranes consistently produced higher flux and greater conversion of heat to permeate flow.

For future membrane design, the following guidance is suggested to improve MD performance:

- Thin scrim support with wider accessible spaces to the membrane surface should yield further flux improvements,
- Hydrophobicity is essential for MD operation, but was not found to link to flux as strongly as other physical features,
- Structures of the composite membrane, i.e, overall thickness, the openness of the support layer, are more important for flux improvement than pore sizes in the ranges tested (0.2 – 1 μm), and
- The geometric structure of the support layer seems to be more important for high flux than that of the porosity, as the flux of scrim backed 0.45 μm membrane was greater than that of the non-woven fabric $M_{mt1.00}$ membrane at the tested flowrates.

## 4. Conclusions

The performance of three new MD membranes in DCMD were assessed based on flux and energy efficiency, and show greater potential for use in desalination processes than do the traditional microfiltration membranes. The new PTFE membranes achieved a significantly higher flux and had better energy efficiency than the MF membranes under the same conditions.

The contact angles of the new membranes were in the range of 140-160°, which are 1.5 times that of $M_{p0.30}$ and 1.25 times that of $M_{mt1.00}$. Similarly, the LEP of the new membranes were 2 times that of the MF membranes, so the new MD membranes can be used at higher operating pressures without the risk of wetting.

The new membranes also show good salt rejection even under critical conditions. In comparison with the 96% salt rejection rate of $M_{p0.30}$, all PTFE membranes achieved nearly 100% salt rejection rate at a feed velocity of 0.36 m/s and ≤20 kPa.

Mass transfer coefficients were calculated to evaluate the mass transfer efficiency of the process under different conditions. All new PTFE membranes have mass transfer coefficients higher than or similar to that of MF membranes under the same conditions.

The more open support layers of the new membranes increase both flux and energy efficiency. Flux of up to 46 $Lm^{-2}h^{-1}$ was obtained at 80°C, which is comparable to the flux achieved in reverse osmosis systems. This suggests that membranes for a commercially viable MD process are available, and issues around module design and long term operation of the MD process (fouling, wetting) need to be resolved. All experimental results presented here were each measured for a period of four to six hours. Experiments over longer time periods are needed to investigate fouling and wetting issues.

## Acknowledgements

## Nomenclature

| | |
|---|---|
| $a$ | exponent of $r$ |
| $A$ | membrane area |
| $\alpha_1, \alpha_2$ | heat transfer coefficient on hot side and cold side |
| $B$ | geometric factor |
| $b$ | membrane thickness |
| $C$ | mass transfer coefficient |
| $C_f$ | feed bulk concentration |
| $C_{solution}$ | concentration of NaCl |
| $C_p$ | specific heat of water |
| $C_1$ | feed concentration at liquid-vapour interface |
| $\varepsilon$ | membrane porosity |
| $\varepsilon_{surface}$ | surface porosity |
| $H_{latent}$ | latent heat of water vaporisation |
| $\lambda$ | thermal conductivity |
| $\lambda_{air}$ | solid thermal conductivity |
| $\lambda_{solid}$ | air thermal conductivity |
| $N$ | vapour flux |
| $m_{total}$ | mass of membrane with the support layer |
| $m_{support}$ | mass of support layer |
| $P_{gas}$ | gas phase pressure in pores |
| $P_{liquid}$ | pressure of the process liquid |
| $P_{T1}, P_{T2}$ | vapour pressure at $T_1$ and $T_2$ |
| $P_{fi}, P_{fo}$ | vapour pressures at inlet and outlet temperatures of the hot side |
| $P_{pi}, P_{po}$ | vapour pressures at inlet and outlet temperatures of cold side |
| $\rho$ | material density of the active layer |
| $Q_f$ | feed mass flowrate |
| $r_{max}$ | the largest pore size of membrane |
| $r$ | nominal pore size of membrane |
| $\theta$ | contact angle between the solution and the membrane surface |
| $t$ | pore tortuosity |
| $T_p, T_f$ | permeate and feed bulk temperatures |
| $T_{fi}, T_{fo}$ | feed inlet and outlet temperatures |
| $T_1, T_2$ | feed and permeate temperatures at liquid-vapour interface |
| $V$ | volume of active layer |
| $\gamma_l$ | surface tension of the solution |
| $\gamma_0$ | pure water surface tension at 25ºC |

## References

[1] M. Tomaszewska, Membrane Distillation-Examples of Applications in Technology and Environmental Protection, Environmental Studies, 9 (2000) 27.

[2] F. Banat and N. Jwaied, Economic evaluation of desalination by small-scale autonomous solar-powered membrane distillation units, Desalination, 220 (2008) 566.

[3] L. Song, B. Li, K.K. Sirkar, and J.L. Gilron, Direct Contact Membrane Distillation-Based Desalination: Novel Membranes, Devices, Larger-Scale Studies, and a Model, Ind. Eng. Chem. Res., 46 (2007) 2307.

[4] M. Mulder, *Basic Principles of Membrane Technology*. 2nd edn ed. 1996, Dordrecht: Kluwer.

[5] A.M. Alklaibi and N. Lior, Membrane-distillation desalination: Status and potential, Desalination, 171 (2005) 111.

[6] S. Bandini and G.C. Sarti, Concentration of must through vacuum membrane distillation, Desalination, 149 (2002) 253.

[7] L. Martinez-Diez and F.J. Florido-Diaz, Theoretical and experimental studies on desalination using membrane distillation, Desalination, 139 (2001) 373.

[8] J. Phattaranawik, R. Jiraratananon, and A.G. Fane, Heat transport and membrane distillation coefficients in direct contact membrane distillation, Journal of Membrane Science, 212 (2003) 177.

[9] Z. Ding, R. Ma, and A.G. Fane, A new model for mass transfer in direct contact membrane distillation, Desalination, 151 (2003) 217.

[10] J. Phattaranawik, R. Jiraratananon, and A.G. Fane, Effect of pore size distribution and air flux on mass transport in direct contact membrane distillation, Journal of Membrane Science, 215 (2003) 75.

[11] M.M. Teoh and T.-S. Chung, Membrane distillation with hydrophobic macrovoid-free PVDF-PTFE hollow fiber membranes, Separation and Purification Technology, In Press, Corrected Proof.

[12] S. Al-Obaidani, E. Curcio, F. Macedonio, G. Di Profio, H. Al-Hinai, and E. Drioli, Potential of membrane distillation in seawater desalination: Thermal efficiency, sensitivity study and cost estimation, Journal of Membrane Science, 323 (2008) 85.

[13] G.W. Meindersma, C.M. Guijt, and A.B. de Haan, Desalination and water recycling by air gap membrane distillation, Desalination, 187 (2006) 291.

[14] M. Qtaishat, T. Matsuura, B. Kruczek, and M. Khayet, Heat and mass transfer analysis in direct contact membrane distillation, Desalination, 219 (2008) 272.

[15] S. Bonyadi and T.S. Chung, Flux enhancement in membrane distillation by fabrication of dual layer hydrophilic-hydrophobic hollow fiber membranes, Journal of Membrane Science, 306 (2007) 134.

[16] K.W. Lawson and D.R. Lloyd, Membrane distillation, Journal of Membrane Science, 124 (1997) 1.

[17] R.W. Schofield, A.G. Fane, and C.J.D. Fell, Gas and vapour transport through microporous membranes. I. Knudsen-Poiseuille transition, Journal of Membrane Science, 53 (1990) 159.

[18] M.N. Chernyshov, G.W. Meindersma, and A.B. de Haan, Modelling temperature and salt concentration distribution in membrane distillation feed channel, Desalination, 157 (2003) 315.

[19] W.T. Hanbury and T. Hodgkiess, Membrane distillation - an assessment, Desalination, 56 (1985) 287.

[20] M. Gryta, M. Tomaszewska, and A.W. Morawski, Membrane distillation with laminar flow, Separation and Purification Technology, 11 (1997) 93.

[21] R. Mishra, S.P. Tripathy, D. Sinha, K.K. Dwivedi, S. Ghosh, D.T. Khathing, M. Muller, D. Fink, and W.H. Chung, Optical and electrical properties of some electron and proton irradiated polymers, Nuclear Instruments and Methods in Physics Research Section B: Beam Interactions with Materials and Atoms, 168 (2000) 59.

[22] Y. Luo, Y. Liu, and Q. Yu, Influence of glow discharge plasma treatment on vapor-induced response of poly(vinylidene fluoride)-carbon black composite thin films, Thin Solid Films, 515 (2007) 4016.

[23] N. Sghaier, M. Prat, and S. Ben Nasrallah, On the influence of sodium chloride concentration on equilibrium contact angle, Chemical Engineering Journal, 122 (2006) 47.

[24] R. Tuckermann, Surface tension of aqueous solutions of water-soluble organic and inorganic compounds, Atmospheric Environment, 41 (2007) 6265.

[25] M. Matheswaran, T.O. Kwon, J.W. Kim, and I. Moon, Factors Affecting Flux and Water Separation Performance in Air Gap Membrane Distillation, Journal of Industrial and Engineering Chemistry, 13 (2007) 965.

[26] M.C. Garcia-Payo, C.A. Rivier, I.W. Marison, and U. von Stockar, Separation of binary mixtures by thermostatic sweeping gas membrane distillation: II. Experimental results with aqueous formic acid solutions, Journal of Membrane Science, 198 (2002) 197.